Exchange and correlation in molecular wire conductance: non-locality is the key

Jeremy S. Evans, Oleg A. Vydrov, and Troy Van Voorhis

Department of Chemistry

Massachusetts Institute of Technology

77 Massachusetts Ave.

Cambridge, MA 02139 USA

Abstract

We study real-time electron dynamics in a molecular junction with a variety of approximations to the electronic structure, toward the ultimate aim of determining what ingredients are crucial for the accurate prediction of charge transport. We begin with real-time, all-electron simulations using some common density functionals that differ in how they treat long-range Hartree-Fock exchange. We find that the inclusion or exclusion of non-local exchange is the dominant factor determining the transport behavior, with all semilocal contributions having a smaller effect. In order to study non-local correlation, we first map our junction onto a simple Pariser-Parr-Pople (PPP) model Hamiltonian. The PPP dynamics are shown to faithfully reproduce the all-electron results, and we demonstrate that non-local correlation can be readily included in the model space using the generator coordinate method (GCM). Our PPP-GCM simulations suggest that non-local correlation has a significant impact on the I-V character that is not captured even qualitatively by any of the common semilocal approximations to exchange and correlation. The implications of our results for transport calculations are discussed.

I. INTRODUCTION

Experiments in the past two decades have examined the unique electron transport properties of single-molecule electronic devices[1–31] generating significant theoretical interest. Landauer and Büttiker provided the first qualitatively correct description of single-molecule transport in terms of molecular conductance channels weakly coupled to scattering states in the metal leads[32–36]. Although the model was originally described in a one-electron framework, the nonequilibrium Green's function (NEGF) method allows one to derive a Landauer-like expression for the exact many-particle system[37]. The difficulty of obtaining the exact NEGF subsequently led to numerous attempts to approximate transport using the NEGF in conjunction with semiempirical[38,39], *ab initio*[40], density functional theory (DFT)[41–48], and model Hamiltonian[49–51] methods. Such approximate NEGF methods currently dominate the literature on single-molecule conductance calculations.

Recently, an alternative microcanonical prescription for describing electron transport has been proposed[52,53]. Here, the entire junction (molecule+leads) begins in equilibrium and one monitors the *real-time response* of the junction to a time-dependent applied bias. The benefit of this framework is that it only requires the time-dependent *density* - as opposed to the full NEGF - to describe the direct current response exactly[52,53]. Further, the exact density is in principle available from time-dependent DFT (TDDFT)[54] making a microcanonical TDDFT approach to conduction an attractive possibility. To date, this framework has been applied both formally[52,53,55] and practically[56–58] in electron transport simulations.

We have previously used real-time TDDFT to study transport in molecular wires using common approximations to the exchange-correlation (xc) functional[59,60]. We have demonstrated, in agreement with several other studies[61–66], the sensitivity of both spin and charge currents to the choice of xc functional. Unfortunately, common approximations in TDDFT do not form a convergent hierarchy, so that it is not possible to say with certainty that one functional gives uniformly better results than another. Thus, the wide variety of predictions obtainable with standard TDDFT makes it practically impossible to identify which functionals, if any, give an accurate description of transport. This ambiguity is particularly acute given that simulations and experiment in this field often disagree by one to two orders of magnitude[62,64]. The situation can be ameliorated by using wavefunction-based techniques[40], but because the microcanonical picture requires such calculations be performed on the en-

tire molecule+leads system - often containing several hundred atoms - correlated *ab initio* investigations along these lines are simply not feasible. One is thus left with significant uncertainty as to the best way to simulate electron transport in molecular junctions.

In this article, we critically examine a number of approximate microcanonical simulations in order to determine which ingredients are required to obtain electron transport dynamics. For simplicity, we focus on a single model junction (see Fig 1). First, we simulate the conductance using a variety of semilocal and hybrid density functionals and find that the predicted current-voltage curves depend *only* on the fraction of non-local Hartree-Fock exchange included in the functional. The presence or absence of semi-local exchange or correlation has a negligible effect on the system at any bias. This is consistent with the fact that, at zero bias, the resistance only depends on the infinite-ranged part of the xc potential[62,67]. In order to assess the impact of non-local wavefunction-based correlation on transport, we first map our TDDFT results on to a Pariser-Parr-Pople (PPP) model Hamiltonian. We then employ the generator coordinate method (GCM) to rapidly incorporate non-local correlation within the model space. We find that non-local correlation significantly increases the transport gap and can even increase the charge currents in the ballistic regime. This behavior is not reproduced by any of the semilocal xc functionals we have tested. We therefore conclude that, at a fundamental level, non-locality is required in both the exchange *and* correlation functionals if one wants to obtain an accurate description of transport. The article concludes with some discussion of the physical implications of these results.

II. CONDUCTANCE IN A MODEL JUNCTION

All the calculations presented in this article concern the model junction depicted in Figure 1. This molecular wire has been designed to mimic the lead-molecule-lead geometries typically used in experiments. The leads are represented by long conjugated *trans*-polyenes, containing 48 carbon atoms each. The molecular "device" is a *trans*-butadiene residue, connected to the leads via two saturated CH_2 segments. The system is designed in such a way that the coupling of the molecular device to the leads is rather weak, because the conjugation is interrupted by the CH_2 groups, leading to poor overlap of the π orbitals. Although the chain of C–C σ-bonds is not interrupted, the electrons in the σ-orbitals are typically much less mobile.

In order to model the conductance of the junction, we use the "microcanonical" picture of transport[52,53]. We first determine the ground state of the entire leads+molecule junction at the desired level of theory (e.g. DFT or model Hamiltonian). Then, at time $t = 0$ the wire is subjected to a bias potential of the form shown in Figure 1, which pushes the system out of equilibrium. We then monitor the difference between the number of charges on the left and right leads, $N(t) \equiv \frac{1}{2}(N_L(t) - N_R(t))$, as a function of time using any of a variety of methods (e.g. TDDFT) for real time electron propagation. We note that a method like TDDFT, which in principle yields the exact time-dependent density, can give the exact $N(t)$[52,53].

$N(t)$ contains significant information about the dynamical response of the junction - including impedance[56] and counting statistics[59]. However, for the purposes of this article, we will be most interested in the steady state conductance of the junction, which is also the aim of NEGF techniques. Because our system is closed, any current can only last a finite amount of time - a finite current acting for an infinite amount of time would result in an infinite number of electrons being transferred. Thus, we can never obtain a true current-carrying steady state in our microcanonical simulations. However, in running these simulations one empirically finds that $N(t)$ typically behaves as shown in Figure 2. After some transient relaxation time, the current, $I = \frac{dN}{dt}$, settles down to a relatively constant value, as shown by the linear fit between 1 and 5 fs. As long as the leads are chosen to be large enough, it is only at much longer times that the current through the wire reverses itself (e.g. around 15 fs in Figure 2). The primary limitation here is numerical: computationally one is limited to some maximum system size, which leads to a finite lifetime for the quasi-steady state, and ultimately leads to statistical uncertainty in the fitted current. For example, in Figure 2 one would obtain a slightly different current if one fitted from 5 fs to 10 fs than if one fitted from 1 fs to 5 fs and neither result could be considered wrong. It has been shown recently[57,59,68] that, with existing computational resources, these numerical uncertainties can be minimized so that the currents obtained in this microcanonical picture agree essentially quantitatively with the true steady state currents. In particular, for the wire studied here we have verified that if the size of the leads is reduced by half the quasi-steady state current is unaffected. The quasi-steady state survives for a shorter period of time, and the statistical uncertainties are concomittantly larger, but the fitted currents are consistent for shorter leads.

In order to probe the current-voltage behavior, we employ a straightforward scheme: we apply a series of voltage biases of different magnitudes, V. For each bias, we propagate

the electrons to obtain $N(t)$. From the quasi-steady state current, we extract I. Finally, an $I-V$ plot is obtained by plotting the values of I thus obtained against the applied bias. This entire procedure is illustrated in Figure 3. At this point it is important to realize that the only *uncontrolled* approximation we make in this procedure relates to the level of electronic structure theory we use to determine and propagate the initial state. The focus of what follows, then, is the impact of approximations to the electronic structure on the predicted currents. In particular, we will focus on determining the correct I-V curve for our model wire and establish what level of theory one needs to employ to get the right answer.

III. REAL-TIME DENSITY FUNCTIONAL CONDUCTANCE SIMULATIONS

First, we simulate the conductance of our junction using direct real time TDDFT propagation of the electron density.[56–58,69] The details of our implementation are presented elsewhere.[59,60] Briefly, our algorithm integrates the time-dependent Kohn-Sham equations

$$i\frac{\partial}{\partial t}\psi_i^{KS}(t) = \hat{H}_{KS}[\rho(t)]\psi_i^{KS}(t) \tag{1}$$

in a Gaussian basis using a second-order Magnus propagator implemented in a development version of the Q-Chem software package.[70] As has been done previously, the bias potential is defined using the Löwdin partition scheme, multiplying the partitioning functions by $+V/2$ for atoms in the source lead and $-V/2$ for atoms in the drain. The real-time scheme has the advantage that it provides a rigorous prediction of currents at any bias, whereas the NEGF-DFT techniques[47,48,71] are only formally correct for the near-equilibrium low bias case.

All practical DFT methods for molecular conductance rely on common approximations to the exchange-correlation (xc) energy. The particular choice of the xc functional has been shown to dramatically affect the results of conductance calculations.[64–66,72–74] This existing work has primarily been focused on the low-bias behavior, but two important conclusions can be drawn. First, the self-interaction error (SIE) present in commonly employed local and semilocal xc functionals is extremely harmful for conductance simulations. As a direct consequence of SIE, semilocal functionals erroneously predict metallic transport even in insulating molecules in weak contact with the leads[64,66,74]. At the same time, it can be shown that at zero bias the xc contribution to the conductance depends only on the induced

shift in v_{xc} infinitely deep in the leads.[62,67] For a semi-local functional, this shift must be zero because the density deep in the leads is unaffected by the bias. Thus, at low bias, one expects a semilocal correction to v_{xc} to have negligible effect on the transport. In order to address these issues, we have performed real-time TDDFT simulations on the model junction with a variety of functionals that differ in the ways they incorporate non-locality and SIE.

For the test system shown in Fig. 1 and using the methodology described in Section II, we compute the I-V curves using four different electronic structure methods: 1) the local density approximation (LDA) 2) a global hybrid of LDA with 50% of the Hartree-Fock-type exchange, which we call "Half&Half" 3) Hartree-Fock (HF) theory and 4) long-range corrected LDA (LC-LDA) which combines the short-range LDA exchange[75,76] with the long-range HF exchange. In LC-LDA, the standard error function is used to split the Coulomb operator into short- and long-range parts, and the range-separation parameter $\omega = 0.5$ Bohr^{-1} is used, which has been shown to work well in many cases.[77,78] The LDA, Half&Half, and LC-LDA xc functionals all include the uniform electron gas correlation functional of Vosko, Wilk and Nusair[79] commonly known as VWN5.

We have optimized the geometry of the junction with B3LYP/6-31G(d). To save time in the conductance simulations, most of our calculations use the minimal STO-3G basis set for the leads and a larger 6-31G(d) basis set for the molecular device and the CH_2 groups. Since our model system does not directly simulate any real-world experimental setup, the minimal basis set should suffice for the description of the leads, which simply serve as a source and a drain of electrons. To assess the effect of the choice of the basis set for the leads, we have performed a few calculations using 6-31G(d) for the entire system and compared them to the calculations using the mixed basis described above. The results, given in Fig. 4, show that the qualitative shapes of the I-V curves are not affected by the choice of the leads' basis set. As we replace 6-31G(d) by STO-3G on the leads, we observe a decrease in the current at larger voltages. This can be explained by the fact that the STO-3G basis set is more restricted and less diffuse, which effectively results in weaker coupling.

Fig. 5 compares the I-V curves obtained with four electronic structure methods. LDA predicts a nonzero current even for very small applied voltages ($V \approx$0.1 a.u.). The Half&Half hybrid gives nonzero average current only for $V > 0.2$ a.u. HF and LC-LDA yield nonzero current only for $V > 0.4$ a.u. The I-V curve obtained with LC-LDA is very similar to the HF result, both qualitatively and quantitatively. These results are consistent with the band

gap predictions for an *isolated* butadiene molecule obtained with the various functionals. LDA predicts a very small gap (0.15 a.u.), Half&Half predicts a much larger gap (0.29 a.u.), and HF and LC-LDA predict the largest gaps (0.44 and 0.42 a.u., respectively). One expects this, because in both situations the reduction of the gap is linked to the presence of SIE in the approximate exchange correlation functionals.[64,80–82]

Fig. 5 clearly illustrates a well-known[64] problem of LDA: in the weakly-coupled limit, LDA gives too large currents at low voltage biases. This problem is attributed to SIE and lack of the proper derivative discontinuity. The Half&Half hybrid yields an I-V curve that is shifted halfway in-between the LDA and HF curves (see Fig. 5). This is expected since the Half&Half exchange functional is a linear combination of LDA and HF exchange. LC-LDA hybrid combines LDA and HF in a very different way, preserving the correct long-range behavior of the exchange potential. As evidenced by the results in Fig. 5, this correct long-range behavior is crucial for the description of the electronic transport in a molecular device weakly coupled to the leads. Finally, we note that LC-LDA includes local correlation, whereas HF has none. Inclusion of local correlation appears to have very little effect on the conductance at any bias. Taken together, these observations essentially extend the conclusions of Refs.62,67 to finite bias: at any value of V it is only the *non-local* portion of the xc functional that influences the charge transport. In commonly used functionals, only the exchange has a non-local component, and so the exchange plays a decisive role in the transport predictions

IV. MODEL HAMILTONIAN CONDUCTANCE SIMULATIONS

A. The PPP Model Hamiltonian

Because the conductance curves show such a strong variability with the choice of xc functional, it is not possible to conclusively determine the correct form of the I-V curve from the data above. Among the four methods represented in Fig. 5, one might consider the LC-LDA and HF results to be the most realistic since HF and LC-LDA are free (or nearly free) of SIE. But neither of these include any effects of non-local correlation, and it is entirely possible that the effects of non-local correlation counteract all or part of the non-local exchange contribution. To put it another way, it is possible that a semi-local functional

might actually give a better prediction through cancellation of errors between SIE and the missing part of the correlation energy. To settle this uncertainty, one would like to perform wavefunction-based simulations of the conductance. Unfortunately, with commonly used quantum chemistry techniques (e.g. MP2 or CCSD) this is not computationally feasible for a junction of this size. However, if we first map the dynamics onto a model Hamiltonian we can vastly reduce the number of degrees of freedom, making highly accurate wavefunction predictions possible.

Toward this end, we attempt to reproduce the conductance results of the full TDDFT and TDHF dynamics with those generated by the Pariser-Parr-Pople (PPP)[83–86] model. PPP is an effective tool for modeling charge transport in π-conjugated systems[38,39,87–89]. Further, we have recently shown[60] that, given the proper parameters, PPP can do an excellent job of reproducing the real-time conduction predictions obtained in more sophisticated TDDFT simulations.

In the PPP picture, one models the π electrons by including only the p_z orbitals on each carbon atom in the conjugated chain. Thus, for our junction we will have $N = 48+4+48 = 100$ orbitals in the model space. The PPP Hamiltonian is:

$$\hat{H} = -\sum_{\substack{j=1 \\ \sigma=\uparrow,\downarrow}}^{N-1} \beta_{jj+1} \left(\hat{c}^{\dagger}_{j\sigma} \hat{c}_{j+1\sigma} + \hat{c}^{\dagger}_{j+1\sigma} \hat{c}_{j\sigma} \right) - \sum_{jk}^{N} \Gamma_{jk} \hat{n}_j + \frac{1}{2} \sum_{jk} \Gamma_{jk} \hat{n}_j \hat{n}_k, \tag{2}$$

$$\Gamma_{j,k} = \left(r_0 \left| j-k \right| + \frac{1}{g} \right)^{-1}, \qquad \hat{n}_j \equiv \left(\hat{c}^{\dagger}_{j,\uparrow} \hat{c}_{j,\uparrow} + \hat{c}^{\dagger}_{j,\downarrow} \hat{c}_{j,\downarrow} \right).$$

The three terms in Eq. 2 correspond to electron hopping between sites, electron-nuclear attraction and electron-electron repulsion, respectively. We set $r_0 = 2.647$, $g = 0.55$ and fix the hopping parameter $\beta_{j,j+1}$ to the constant value $\beta_0 = 0.16$ as long as j and $j+1$ both belong to either a lead or the molecule. These values have been shown to reproduce the TDDFT predictions of both charge and spin dynamics of conjugated carbon chains quite well[60]. Meanwhile, if j belongs to the molecule and $j+1$ to a lead (or vice versa) the hopping parameter is reduced to a value of $\beta_{Gap} = 0.024$ to reflect the reduced overlap between the p_z orbitals separated by a saturated CH_2 unit. Reasonable variations in the magnitude of of β_{Gap} have little effect on the shape of the I-V curve, but have a significant impact on the magnitude of the overall current.

B. Non-local Exchange in the PPP model

In order to be sure that the PPP model contains the proper physics, one would like to obtain PPP-based models that reproduce the different TDDFT results above (LDA, Half&Half, HF, LC-LDA). The PPP-HF model is easiest to develop. One first approximates the wavefunction as a Slater determinant, $\Psi(t)$, constructed out of N occupied spin orbitals $\psi_i(t)$. These orbitals are written as linear combinations of the localized p_z orbitals:

$$\psi_i(t) = \sum_\alpha c_i^\alpha(t) p_z^\alpha. \tag{3}$$

After some algebra (see, for example,Ref. 60) one finds the orbital coefficients, $\mathbf{c}_i$, satisfy

$$i\dot{\mathbf{c}}_i(t) = \mathbf{F}[\mathbf{c}]\mathbf{c}_i(t) \tag{4}$$

with the effective one-electron Hamiltonian

$$F_{ij}[\mathbf{c}] = h_{ij} + \sum_k^N \Gamma_{jk} P_{kk} \delta ij - \frac{1}{2}\Gamma_{ij} P_{ij} \tag{5}$$

were $\mathbf{P} \equiv 2\sum_i^{occ} \mathbf{c}_i \mathbf{c}_i^\dagger$ is the noninteracting one particle density matrix. The first term in Eq. 5 corresponds to the bare one-body Hamiltonian, while the second and third terms represent Coulomb and exchange interactions, respectively. The PPP-TDHF equations can be solved in strictly analogous fashion to the TDDFT equations in the previous section. To obtain currents, we apply a bias using the Löwdin partition functions, propagate the orbitals via Eq. 4 using Magnus integration and obtain a current from the quasi-steady state slope of $N(t)$.

In order to obtain analogs for the various density functionals within the PPP model, we begin with the working hypothesis that only the non-local part of the xc functional matters. On this basis, one would conclude that LDA - which has no non-local xc part - should be represented by an effective Hamiltonian of the form of Eq. 5 with the non-local exchange term removed (PPP-LDA). Continuing along this line of thought, one obtains PPP-Half&Half by multiplying the exchange term by $\frac{1}{2}$ and PPP-LC by multiplying Γ_{jk} in the exchange term by $\mathrm{erf}(0.5 r_{jk})$. On the one hand, these are drastic approximations because one neglects all the effects of local exchange and correlation. On the other hand, this picture is certainly consistent with the results of the previous section and previous work[60,62,64,66,67,74] and so one anticipates it may be effective.

Fig. 6 compares the I-V curves calculated using the PPP models described above with those calculated using TDDFT with various functionals. We note that, like the TDDFT methods, the PPP results show a gap between $V = 0$ and the first appearance of current. Furthermore, the change in the size of gap with the amount of exact exchange mirrors the result calculated with all-electron methods. We find the largest conductance gap with 100% exact exchange methods (HF) and the smallest gap with methods that include no exact exchange (LDA). The 50% exact exchange methods (Half&Half) show an intermediate gap. Finally, like the all electron results, the long range corrected method (PPP-LC) is quantitatively very similar to PPP-HF. We note that in each case, the all electron methods show a monotonic increase in current after turn-on, while the PPP results tend to saturate. This difference is likely due to the absence of any orbitals besides the p_z orbitals in the PPP calculations. While unimportant at low biases, the σ orbitals will play a significant role at higher bias, leading ultimately to a discrepancy between the methods for large values of V. Finally, we note that the quantitative differences between the PPP and TDDFT(TDHF) turn-on voltages could be adjusted somewhat by changing the electron repulsion parameter g.

Overall, the strong qualitative agreement between the PPP model and the TDDFT results points toward two conclusions. First, it provides further evidence that non-local exchange dominates the conductance behavior of these functionals. We have completely neglected local xc-contributions to obtain the PPP-LDA, PPP-Half&Half and PPP-LC results. The fact that these are even remotely correct suggests that the local contributions are small compared to the dominant HF exchange contribution. Second, these results strongly suggest that the PPP model, while simple, contains enough physics to describe influence of exchange and correlation on transport in these junctions.

C. Correlated Conductance of the PPP model

Now that we have validated our model Hamiltonian and examined the importance of non-local exchange, we would like to answer the question: what effect does non-local correlation have on the conductance? We will address this point using a time-dependent version of the generator-coordinate method (GCM). The GCM was first introduced by Wheeler and Hill to describe correlation in nuclear matter.[90,91] More recently, the GCM has been used to

make connections between DFT and wavefunction-based approaches to correlation.[92,93] For a time independent problem, the fundamental idea is to write the target wavefunction, Ψ, as a linear transformation of a continuous set of states:

$$|\Psi\rangle = \int c(\eta)|\Phi(\eta)\rangle d\eta. \tag{6}$$

Here $|\Phi(\eta)\rangle$ is some approximate wavefunction and the variable η could be any continuous parameter that deforms Φ. In order to determine the optimal ground state Ψ, one solves the Wheeler-Hill (WH) equation for the coefficients, $c(\eta)$:

$$\int \left[H(\eta;\eta') - ES(\eta;\eta')\right] c(\eta')d\eta' = 0 \tag{7}$$

where $H(\eta;\eta') \equiv \langle\Phi(\eta)|\hat{H}|\Phi(\eta')\rangle$ and $S(\eta;\eta') \equiv \langle\Phi(\eta)|\Phi(\eta')\rangle$ are the matrix representations of the Hamiltonian and overlap, respectively. The GCM can also be used to describe correlated dynamics.[93] Here one writes the time-dependent GCM wavefunction, $\Psi(t)$, as

$$|\Psi(t)\rangle = \int c(t;\eta)|\Phi(\eta)\rangle d\eta \tag{8}$$

where the time evolution of the coefficients, $c(t;\eta)$, is governed by the time-dependent WH (TD-WH) equation

$$\int \left(H_b(\eta;\eta') - i\frac{\partial}{\partial t}S(\eta;\eta')\right) c(t;\eta')d\eta' = 0. \tag{9}$$

The physical picture in the GCM model is that, while the approximate $\Phi(\eta)$ may not provide an accurate picture of either the ground state Ψ or $\Psi(t)$, one expects that the set of all $\Phi(\eta)$ will provide a *good basis* for expanding the true solutions. For example, while each $\Phi(\eta)$ might be a single determinant, the correlated state Ψ can in principle involve an *infinite* number of determinants.

In practice, Eq. 7 is discretized by choosing a fixed set of deformations $\{\eta_i\}$. The WH equation is then equivalent to a nonorthogonal configuration interaction (CI) calculation in the space spanned by the states $|\Phi_i\rangle \equiv |\Phi(\eta_i)\rangle$:

$$\mathbf{H}\cdot\mathbf{c} = E\mathbf{S}\cdot\mathbf{c}. \tag{10}$$

The Hamiltonian matrix, $\mathbf{H}$, has elements $H_{ij} \equiv \langle\Phi(\eta_i)|\hat{H}|\Phi(\eta_j)\rangle$ and the overlap matrix , $\mathbf{S}$, is defined by $S_{ij} \equiv \langle\Phi(\eta_i)|\Phi(\eta_j)\rangle$. Meanwhile, the TD-WH equation can be rearranged to:

$$i\frac{\partial}{\partial t}\mathbf{c}(t) = \mathbf{S^{-1}}\cdot\mathbf{H}\cdot\mathbf{c}(t) \tag{11}$$

which can be integrated using standard numerical integration techniques. Like any CI method, the GCM is exact if enough discrete deformations are included. In practice, the GCM with even a few η_i can describe correlated ground state properties extremely well.[92]

In our case, we want to describe the wavefunction as a function of two obvious deformation parameters: potential bias (V) and time (τ). Thus we write the time dependent GCM wavefunction in terms of the group parameter $\eta = \{V, \tau\}$:

$$|\Psi(t)\rangle = \int c(t;\eta)|\Phi(\eta)\rangle d\eta = \int c(t;V,\tau)|\Phi(V,\tau)\rangle dV d\tau. \tag{12}$$

Here, $|\Phi(V,\tau)\rangle$ is an approximate (e.g. HF or DFT) wavefunction propagated for a time τ in a potential bias V. We can then determine the ground state in the absence of the potential by the analogous WH equation:

$$\int \left(H(V,\tau;V',\tau') - ES(V,\tau;V',\tau')\right) c(0;V',\tau') dV' d\tau' = 0. \tag{13}$$

Here $H(V,\tau;V',\tau') \equiv \langle\Phi(V,\tau)|\hat{H}|\Phi(V',\tau')\rangle$ and $S(V,\tau;V',\tau') \equiv \langle\Phi(V,\tau)|\Phi(V',\tau')\rangle$. Given that the system starts in the ground state (Eq. 13) we can also follow the time evolution in the presence of a bias potential, V_b, by solving the TD-WH equation:

$$\int \left(H_b(V,\tau;V',\tau') - i\frac{\partial}{\partial t} S(V,\tau;V',\tau')\right) c(t;V',\tau') dV' d\tau' = 0, \tag{14}$$

where $H_b(V,\tau;V',\tau') \equiv \langle\Phi(V,\tau)|\hat{H} + \hat{V}_b|\Phi(V',\tau')\rangle$ is the matrix representation of the Hamiltonian in the presence of the bias. To be clear, in the above equation t and V_b correspond to the physical time and physical bias potential in the simulation, while V, τ, V' and τ' correspond to the deformation parameters used as generator coordinates. It is important to recognize that this realization of TD-GCM does not assume that TDDFT or TDHF provides a good picture for the dynamics. Rather, one assumes that the TDDFT/TDHF wavefunctions with different biases and evolved for different times provide a good *basis* for expanding the true time-dependent wavefunction. In this respect, the present formulation of time dependent GCM is somewhat more flexible than previous versions.[93] Like the canonical version, the TD-GCM is exact if enough determinants are included in the expansion.

TD-GCM provides a powerful and flexible means of examining explicit non-local correlation effects on electron dynamics. Here, we perform microcanonical transport simulations using the above TD-GCM formalism as follows. 1) The integral form for the wavefunction (Eq. 12) is discretized in both time, τ_i, and potential, V_j. Because there are 100 orbitals

and 50 electrons in our PPP model of the junction, a complete CI calculation would require approximately $\binom{100}{50}^2 \approx 10^{28}$ determinants. Clearly it is impossible to include even a small fraction of these states in our TD-GCM space. At this point, the choice of basis states in TD-GCM becomes significant: the TDDFT evolution used to generate the basis states naturally selects only configurations that are important to the dynamics. In practice, we find that ≈ 30 time points and ≈ 300 biases (for a total of only $30 \times 300 \approx 10^4$ determinants) gives essentially converged results. We also find that faster convergence is achieved if different potentials are applied to the $\uparrow$ and $\downarrow$ electrons ($V_j^{\uparrow} \neq V_j^{\downarrow}$) in a spin-unrestricted fashion. We suspect this relates to the difficulty of representing open shell singlet configurations in terms of closed shell basis states. 2) We solve for the lowest eigenvector of $\mathbf{H}$ (Eq. 10) and use this as the initial state for all subsequent propagation. To solve the eigenvalue problem, we first transform to an orthogonal basis by pre- and post-multiplying by $\mathbf{S}^{-1/2}$. 3) The time evolved coefficients, $\mathbf{c}(t)$, under the bias, V_b, are obtained from Eq. 11 by constructing the time evolution operator $\mathbf{U}(t) \equiv exp\left[-i(\mathbf{H} + \mathbf{V_b})t\right]$ in the orthogonalized basis. 4) Using the thus computed $\mathbf{c}(t)$ one computes the time evolution of $N(t)$. A linear fit of $N(t)$ versus t in the quasi-steady state region gives the predicted current I for the present bias. 5) Steps 3&4 are repeated for several voltages to generate an I-V curve.

Using the above prescription for the PPP model of the junction in Figure 1, we obtain the GCM results shown in Figure 7. For comparison, the PPP results from Fig. 6 are also reproduced in Figure 7. The GCM results in this figure were obtained from a basis of 600 potentials with $-1 < \frac{1}{2}(V^{\uparrow} + V^{\downarrow}) < 1$, $-0.1 < \frac{1}{2}(V^{\uparrow} - V^{\downarrow}) < 0.1$ and 32 times, τ, with $-24\ fs < \tau < 24\ fs$. There are a total of 19,200 determinants, but similar results could be obtained with the GCM space is reduced by 50%. Further, the propagation in this example was performed with PPP-HF, although again similar results could be obtained with other functionals. The striking feature of the TD-GCM results is that the transport gap is actually somewhat *larger* than that that predicted by TDHF. This trend is opposite the effect predicted by any of the semilocal xc functionals. Those functionals tend to significantly *narrow* the gap if less than 100% long range exact exchange is included, and have negligible impact otherwise. Thus, none of the commonly used functionals provides an appropriate treatment of electron correlation in these junctions. This trend in the transport gap is at odds with the typical expectation for band gaps: usually, while semilocal functionals severely underestimate gaps[81,82], 100% non-local exchange overestimates them[94]. We attribute the

unusual behavior in this case to the fairly large on-site repulsion value of $g = .55\ a.u.$ in these polyethylene wires, which places the system very near a Mott insulator transition[95]. In a Mott insulator, every site becomes strictly singly occupied in the ground state and only the spin on each site varies: $|\uparrow\downarrow\uparrow ...\rangle$. In order to induce transport in the Mott regime, one site must become doubly occupied, which incurs a penalty of g relative to the all-singly occupied configuration. Thus, if our system were a true Mott insulator the gap would be $g = .55\ a.u.$, which is actually quite close to the transport gap predicted in the GCM calculations. Thus we conclude that, in the GCM calculations, the transport gap is larger because the correlated ground state is more Mott-like than the HF one.

The second obvious feature of the GCM results is that after the gap is overcome, the currents are somewhat larger in the correlated calculations. We note that there is a fair bit of uncertainty in the correlated currents because the N vs. t plots for GCM are much less linear than they are for HF. An example of this is illustrated in Fig. 8. Clearly, the GCM results show long-time oscillation superimposed on a generally linear trend. The persistent oscillation in $N(t)$ might be evidence of a long-lived quasi-bound state on the molecule[96], but we have not been able to verify this possibility. In any case, the variation of $N(t)$ makes precise estimation of the true steady-state current difficult. We have chosen to use the short-time data (e.g. the first 2.5 fs in Fig. 8) to tabulate the currents in Fig. 7, since this avoids any potential complications from finite-size effects at long times. If we had instead chosen to average over a long time interval (e.g. over the first 6 fs in Fig 8) the overall currents would be smaller - similar in magnitude to the HF results, in fact. However, if we fit over the longer interval, the computed GCM transport gap also becomes even larger (.65 a.u.) because the oscillations tend to wash out any directed charge flow when the current is small. Thus, while the GCM result in Fig. 7 should be viewed as somewhat imprecise, one conclusion is unavoidable: nonlocal correlation shifts the I-V curve opposite the direction predicted by semilocal DFT.

V. CONCLUSIONS

In this article we have examined the impact of common approximations to exchange and correlation on the simulation of electron transport through molecular junctions. We use the prototypical device shown in Figure 1 as a model system, and employ the microcanonical

picture of *real-time* electron transport to study the conductance with various approximations to the electronic structure. The microcanonical picture has the advantage that it is in principle exact for any formalism, such as TDDFT, that produces the exact density. Real-time TDDFT simulations with different approximate xc functionals reveal that only the non-local Hartree-Fock exchange has any significant impact on transport - the choice of local functional has only a marginal effect. These observations are consistent with previous results concerning the zero-bias conductance of a junction.[62,67] In order to examine the influence of non-local *correlation* on transport, we first map the molecular junction onto a PPP model Hamiltonian. We demonstrate that appropriately parametrized PPP dynamics provide a reasonably faithful description of the TDDFT charge currents obtained with different xc functionals. Meanwhile, because of the simplicity of the PPP model, the complicated effects of non-local correlation can be easily incorporated using the generator coordinate method. We find that non-local correlation actually tends to widen the transport gap in our model junction, whereas all commonly used approximate xc functionals narrow the gap. Thus, conductance could be something of a worst-case scenario for semilocal xc functionals, which are most successful when there is a partial cancellation between nonlocal exchange and nonlocal correlation. In the particular model studied here, these two nonlocal energy components shift the gap in the *same* direction, so that partial neglect of one of these terms is bound to lead to large errors.

Our work has a number of implications in the ongoing search for accurate methods for predicting molecular electron transport properties. First, our results strongly suggest that most existing approximate functionals significantly overestimate the current in molecular devices because they rely on local approximations. Typical metal-molecule-metal junction experiments are performed in the tunneling regime, which corresponds to the low bias region in this paper. In this situation, nearly all the functionals predict low currents, but the ones with larger transport gaps will produce *exponentially smaller* currents. We find that by far the dominant factor in determining the transport gap is the non-local part of the xc functional. Second, our results show that non-local correlation can also effect the current in the *ballistic* regime, where the bias is large enough to push an electron on or off the molecule. For this specific case, we find that correlation significantly reduces the resistance of the junction (i.e. the current goes up) toward ballistic transport.

Moving forward, our findings suggest several avenues for future research. First, it should

be noted that all our conclusions have been drawn from a single test system. It will be very interesting to see how these results change, or if they change at all, for a more realistic molecular junction such as the Gold-BDT-Gold junction that is used as a common test case of molecular transport. Calculations of this sort are underway in our group. Second, our findings argue for increased investigation of non-local density functionals in conductance simulations. We have here demonstrated that a fully non-local exchange model - as in LC-LDA - can provide a significant improvement in DFT transport predictions. It would be extremely interesting to explore the analogous influence of truly non-local *correlation* methods. For example, one would expect that a method like GW-BSE[97] or EOM-CC[98] should significantly improve DFT transport predictions. A more computationally practical approach might be given by TD current DFT[99,100], where at least some degree of density non-locality can be encoded by the local current.[61,101,102] It is our expectation that investigations along these lines will lead to advances both in the accurate prediction of electron transport and the accurate description of electronic structure using wavefunction- and density-based techniques.

VI. ACKNOWLEDGMENTS

T. V. gratefully acknowledges support from an NSF CAREER award (CHE-0547877) and a Packard Fellowship.

---

[1] T. A. Jung, R. R. Schlittler, J. K. Gimzewski, H. Tang, and C. Joachim, Science **271**, 181 (1996).

[2] L. A. Bumm, J. J. Arnold, M. T. Cygan, T. D. Dunbar, T. P. Burgin, L. Jones, D. L. Allara, J. M. Tour, and P. S. Weiss, Science **271**, 1705 (1996).

[3] M. A. Reed, C. Zhou, C. J. Muller, T. P. Burgin, and J. M. Tour, Science **278**, 252 (1997).

[4] B. C. Stipe, M. A. Rezaei, and W. Ho, Science **280**, 1732 (1998).

[5] G. Leatherman, E. Durantini, D. Gust, T. Moore, A. Moore, S. Stone, Z. Zhou, P. Rez, Y. Liu, and S. Lindsay, Journal of Physical Chemistry B **103**, 4006 (1999), ISSN 1520-6106.

[6] H. Park, J. Park, A. K. L. Lim, E. H. Anderson, A. P. Alivisatos, and P. L. McEuen, Nature

407, 57 (2000), ISSN 0028-0836.

[7] P. G. Collins, M. S. Arnold, and P. Avouris, Science **292**, 706 (2001).

[8] X. D. Cui, A. Primak, X. Zarate, J. Tomfohr, O. F. Sankey, A. L. Moore, T. A. Moore, D. Gust, G. Harris, and S. M. Lindsay, Science **294**, 571 (2001).

[9] P. McEuen, M. Fuhrer, and H. Park, Nanotechnology, IEEE Transactions on **1**, 78 (2002), ISSN 1536-125X.

[10] W. Liang, M. P. Shores, M. Bockrath, J. R. Long, and H. Park, Nature **417**, 725 (2002), ISSN 0028-0836.

[11] J. Park, A. N. Pasupathy, J. I. Goldsmith, C. Chang, Y. Yaish, J. R. Petta, M. Rinkoski, J. P. Sethna, H. D. Abruna, P. L. McEuen, et al., Nature **417**, 722 (2002), ISSN 0028-0836.

[12] P. Avouris, Accounts of Chemical Research **35**, 1026 (2002), ISSN 0001-4842.

[13] J. Kushmerick, J. Lazorcik, C. Patterson, R. Shashidhar, D. Seferos, and G. Bazan, Nano Letters **4**, 639 (2004), ISSN 1530-6984.

[14] X. Xiao, B. Xu, and N. Tao, Nano Letters **4**, 267 (2004), ISSN 1530-6984.

[15] N. Guisinger, M. Greene, R. Basu, A. Baluch, and M. Hersam, Nano Letters **4**, 55 (2004), ISSN 1530-6984.

[16] R. McCreery, Chemistry of Materials **16**, 4477 (2004), ISSN 0897-4756.

[17] K. Kitagawa, T. Morita, and S. Kimura, Journal of Physical Chemistry B **109**, 13906 (2005), ISSN 1520-6106.

[18] R. P. Andres, T. Bein, M. Dorogi, S. Feng, J. I. Henderson, C. P. Kubiak, W. Mahoney, R. G. Osifchin, and R. Reifenberger, Science **272**, 1323 (1996).

[19] R. Martel, T. Schmidt, H. R. Shea, T. Hertel, and P. Avouris, Applied Physics Letters **73**, 2447 (1998).

[20] J. Chen, M. A. Reed, A. M. Rawlett, and J. M. Tour, Science **286**, 1550 (1999).

[21] M. C. Hersam, N. P. Guisinger, J. Lee, K. Cheng, and J. W. Lyding, Applied Physics Letters **80**, 201 (2002).

[22] G. V. Nazin, X. H. Qiu, and W. Ho, Science **302**, 77 (2003).

[23] A. Salomon, D. Cahen, S. Lindsay, J. Tomfohr, V. Engelkes, and C. Frisbie, Advanced Materials **15**, 1881 (2003).

[24] D. I. Gittins, D. Bethell, D. J. Schiffrin, and R. J. Nichols, Nature **408**, 67 (2000), ISSN 0028-0836.

[25] S. Wu, N. Ogawa, G. Nazin, and W. Ho, Journal of Physical Chemistry C **112**, 5241 (2008), ISSN 1932-7447.

[26] N. J. Tao, Nat Nano **1**, 173 (2006), ISSN 1748-3387.

[27] L. Venkataraman, J. E. Klare, C. Nuckolls, M. S. Hybertsen, and M. L. Steigerwald, Nature **442**, 904 (2006), ISSN 0028-0836.

[28] L. Yu, K. Chen, J. Song, J. Wang, J. Xu, W. Li, and X. Huang, Thin Solid Films **515**, 5466 (2007).

[29] C. Livermore, C. H. Crouch, R. M. Westervelt, K. L. Campman, and A. C. Gossard, Science **274**, 1332 (1996).

[30] X. W. Tu, G. Mikaelian, and W. Ho, Physical Review Letters **100**, 126807 (2008).

[31] P. Liljeroth, J. Repp, and G. Meyer, Science **317**, 1203 (2007).

[32] R. Landauer, IBM Journal or Research and Development **1**, 223 (1957).

[33] R. Landauer, Philosophical Magazine **21**, 863 (1970), ISSN 1478-6435.

[34] R. Landauer, Zeitschrift fr Physik B Condensed Matter **21**, 247 (1975).

[35] M. Buttiker, Physical Review Letters **57**, 1761 (1986).

[36] M. Buttiker, Physical Review B **38**, 9375 (1988).

[37] Y. Meir and N. S. Wingreen, Phys. Rev. Lett. **68**, 2512 (1992).

[38] S. Datta, Superlattices and Microstructures **28**, 253 (2000).

[39] T. N. Todorov, Journal of Physics: Condensed Matter **14**, 3049 (2002), ISSN 0953-8984.

[40] P. Delaney and J. C. Greer, Phys. Rev. Lett. **93**, 036805 (2004).

[41] J. Taylor, H. Guo, and J. Wang, Physical Review B **63**, 245407 (2001).

[42] P. Derosa and J. Seminario, Journal of Physical Chemistry B **105**, 471 (2001), ISSN 1520-6106.

[43] Y. Xue, S. Datta, and M. A. Ratner, Chemical Physics **281**, 151 (2002).

[44] T. Tada, M. Kondo, and K. Yoshizawa, The Journal of Chemical Physics **121**, 8050 (2004).

[45] G. C. Solomon, J. R. Reimers, and N. S. Hush, The Journal of Chemical Physics **121**, 6615 (2004).

[46] G. C. Solomon, J. R. Reimers, and N. S. Hush, The Journal of Chemical Physics **122**, 224502 (2005).

[47] M. Brandbyge, J.-L. Mozos, P. Ordejón, J. Taylor, and K. Stokbro, Phys. Rev. B **65**, 165401 (2002).

[48] S.-H. Ke, H. U. Baranger, and W. Yang, Phys. Rev. B **70**, 085410 (2004).

[49] V. Mujica, M. Kemp, A. Roitberg, and M. Ratner, The Journal of Chemical Physics **104**, 7296 (1996).

[50] H. Ness and A. J. Fisher, Physical Review Letters **83**, 452 (1999).

[51] T. Kostyrko and B. R. Buka, Physical Review B **67**, 205331 (2003).

[52] G. Stefanucci and C.-O. Almbladh, EPL (Europhysics Letters) **67**, 14 (2004), ISSN 0295-5075.

[53] M. D. Ventra and T. N. Todorov, Journal of Physics: Condensed Matter **16**, 8025 (2004), ISSN 0953-8984.

[54] E. Runge and E. K. U. Gross, Physical Review Letters **52**, 997 (1984).

[55] K. Burke, R. Car, and R. Gebauer, Physical Review Letters **94**, 146803 (2005).

[56] R. Baer, T. Seideman, S. Ilani, and D. Neuhauser, J. Chem. Phys. **120**, 3387 (2004).

[57] N. Bushong, N. Sai, and M. Di Ventra, Nano Lett. **5**, 2569 (2005).

[58] S. Kurth, G. Stefanucci, C.-O. Almbladh, A. Rubio, and E. K. U. Gross, Phys. Rev. B **72**, 035308 (2005).

[59] C.-L. Cheng, J. S. Evans, and T. V. Voorhis, Physical Review B (Condensed Matter and Materials Physics) **74**, 155112 (2006).

[60] J. S. Evans, C. L. Cheng, and T. Van Voorhis, Phys. Rev. B **78**, 165108 (2008).

[61] N. Sai, M. Zwolak, G. Vignale, and M. D. Ventra, Physical Review Letters **94**, 186810 (2005).

[62] M. Koentopp, K. Burke, and F. Evers, Physical Review B (Condensed Matter and Materials Physics) **73**, 121403 (2006).

[63] S. Kummel, L. Kronik, and J. P. Perdew, Physical Review Letters **93**, 213002 (2004).

[64] C. Toher, A. Filippetti, S. Sanvito, and K. Burke, Phys. Rev. Lett. **95**, 146402 (2005).

[65] S.-H. Ke, H. U. Baranger, and W. Yang, J. Chem. Phys. **126**, 201102 (2007).

[66] C. Toher and S. Sanvito, Phys. Rev. Lett. **99**, 056801 (2007).

[67] M. Koentopp, C. Chang, K. Burke, and R. Car, Journal of Physics: Condensed Matter **20**, 083203 (2008).

[68] N. Sai, N. Bushong, R. Hatcher, and M. D. Ventra, Physical Review B (Condensed Matter and Materials Physics) **75**, 115410 (2007).

[69] X. Qian, J. Li, X. Lin, and S. Yip, Phys. Rev. B **73**, 035408 (2006).

[70] Y. Shao, L. Fusti-Molnar, Y. Jung, J. Kussmann, C. Ochsenfeld, S. T. Brown, A. T. B. Gilbert, L. V. Slipchenko, S. V. Levchenko, D. P. O'Neill, et al., Phys. Chem. Chem. Phys. **8**, 3172 (2006).

[71] A. R. Rocha, V. M. García-Suárez, S. Bailey, C. Lambert, J. Ferrer, and S. Sanvito, Phys. Rev. B **73**, 085414 (2006).

[72] R. Baer, E. Livshits, and D. Neuhauser, Chem. Phys. **329**, 266 (2006).

[73] H. Wang and G. K.-L. Chan, Phys. Rev. B **76**, 193310 (2007).

[74] C. Toher and S. Sanvito, Phys. Rev. B **77**, 155402 (2008).

[75] A. Savin, in *Recent Developments and Applications of Modern Density Functional Theory*, edited by J. M. Seminario (Elsevier, Amsterdam, 1996), pp. 327–357.

[76] P. M. W. Gill, R. D. Adamson, and J. A. Pople, Mol. Phys. **88**, 1005 (1996).

[77] I. C. Gerber and J. G. Ángyán, Chem. Phys. Lett. **415**, 100 (2005).

[78] O. A. Vydrov, J. Heyd, A. V. Krukau, and G. E. Scuseria, J. Chem. Phys. **125**, 074106 (2006).

[79] S. H. Vosko, L. Wilk, and M. Nusair, Can. J. Phys. **58**, 1200 (1980).

[80] J. P. Perdew, R. G. Parr, M. Levy, and J. L. Balduz, Jr., Phys. Rev. Lett. **49**, 1691 (1982).

[81] J. P. Perdew and M. Levy, Phys. Rev. Lett. **51**, 1884 (1983).

[82] L. J. Sham and M. Schluter, Phys. Rev. Lett. **51**, 1888 (1983).

[83] R. Pariser and R. G. Parr, The Journal of Chemical Physics **21**, 466 (1953).

[84] J. A. Pople, Transactions of the Faraday Society **49**, 1375 (1953).

[85] K. Nishimoto and N. Mataga, Zeitschrift Fur Physikalische Chemie Neue Folge **12**, 335 (1957).

[86] N. Mataga and K. Nishimoto, Zeitschrift Fur Physikalische Chemie Neue Folge **13**, 140 (1957).

[87] M. Paulsson and S. Stafstrm, Physical Review B **64**, 035416 (2001).

[88] S. K. Pati, The Journal of Chemical Physics **118**, 6529 (2003).

[89] B. Muralidharan, A. W. Ghosh, and S. Datta, Physical Review B (Condensed Matter and Materials Physics) **73**, 155410 (2006).

[90] D. L. Hill and J. A. Wheeler, Phys. Rev. **89**, 1102 (1953).

[91] J. J. Griffin and J. A. Wheeler, Phys. Rev. **108**, 311 (1957).

[92] K. Capelle, The Journal of Chemical Physics **119**, 1285 (2003).

[93] E. Orestes, K. Capelle, A. B. F. da Silva, and C. A. Ullrich, The Journal of Chemical Physics **127**, 124101 (pages 10) (2007).

[94] J. Paier, M. Marsman, K. Hummer, G. Kresse, I. C. Gerber, and J. G. Ángyán, The Journal of Chemical Physics **124**, 154709 (pages 13) (2006).

[95] M. Imada, A. Fujimori, and Y. Tokura, Rev. Mod. Phys. **70**, 1039 (1998).

[96] G. Stefanucci, Phys. Rev. B **75**, 195115 (2007).

[97] L. Hedin, Phys. Rev. **139**, A796 (1965).

[98] J. F. Stanton and R. J. Bartlett, J. Chem. Phys. **98**, 7029 (1993).

[99] G. Vignale and M. Rasolt, Phys. Rev. Lett. **59**, 2360 (1987).

[100] G. Vignale and W. Kohn, Phys. Rev. Lett. **77**, 2037 (1996).

[101] G. Vignale, C. A. Ullrich, and S. Conti, Phys. Rev. Lett. **79**, 4878 (1997).

[102] M. van Faassen, P. L. de Boeij, R. van Leeuwen, J. A. Berger, and J. G. Snijders, Phys. Rev. Lett. **88**, 186401 (2002).

FIG. 1: Schematic representation of the model system and the voltage bias.

FIG. 2: Number of charges transferred from left to right as a function of time in the model junction. The system begins in the ground state and a bias is applied at time zero. After a transient period of a few hundred attoseconds, a quasi-steady state is achieved. This steady state lasts until the charge in the leads is depleted at around 15 fs. Steady state currents can be obtained from the slope of N vs. t as illustrated by the broken line. These results are with TD-LDA and a voltage bias of 0.2 a.u., but similar physics prevails for all methods in this article.

FIG. 3: By running simulations at several voltages (left) and performing linear fits to the quasi-steady state region for each N versus t curve, a current-voltage plot is obtained (right). These results were obtained with LDA on the model junction. The same prescription is followed to obtain $I-V$ curves for all methods in this article.

FIG. 4: Comparison of the I-V curves obtained using the 6-31G(d) basis set on the entire system with the I-V curves obtained using a mixed basis set (STO-3G on the leads, 6-31G(d) elsewhere).

FIG. 5: The I-V curves computed with four different methods. The STO-3G basis set is used for the leads and 6-31G(d) for the rest of the model system.

FIG. 6: Current-voltage plots calculated using several all electron (left) and PPP (right) methods. Analogous all electron and PPP method pairs are given the same color and line type.

FIG. 7: Current-voltage plots calculated using several PPP methods. The non-local correlation present in the GCM calculations results in qualitative changes in the current.

FIG. 8: Number of electrons transferred in TD-GCM and TDHF calculations at a fixed bias of V=.74 a.u.. The correlated results show persistent oscillations not present in the uncorrelated results.

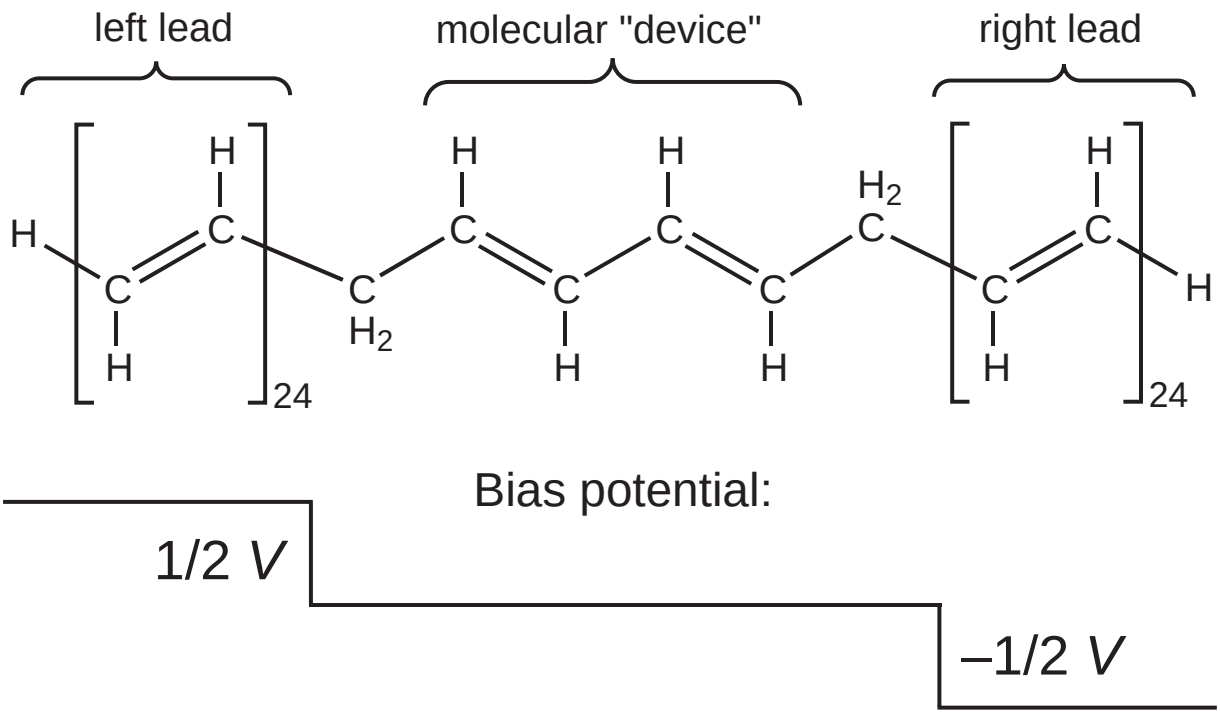
left lead
molecular "device"
right lead
H
H
C
C
H
H
C
C
H
H
C
C
H
H
C
C
H
H
C
C
H
H
C
C
H
H
C
C
H
H
24
24
Bias potential:
1/2 V
–1/2 V

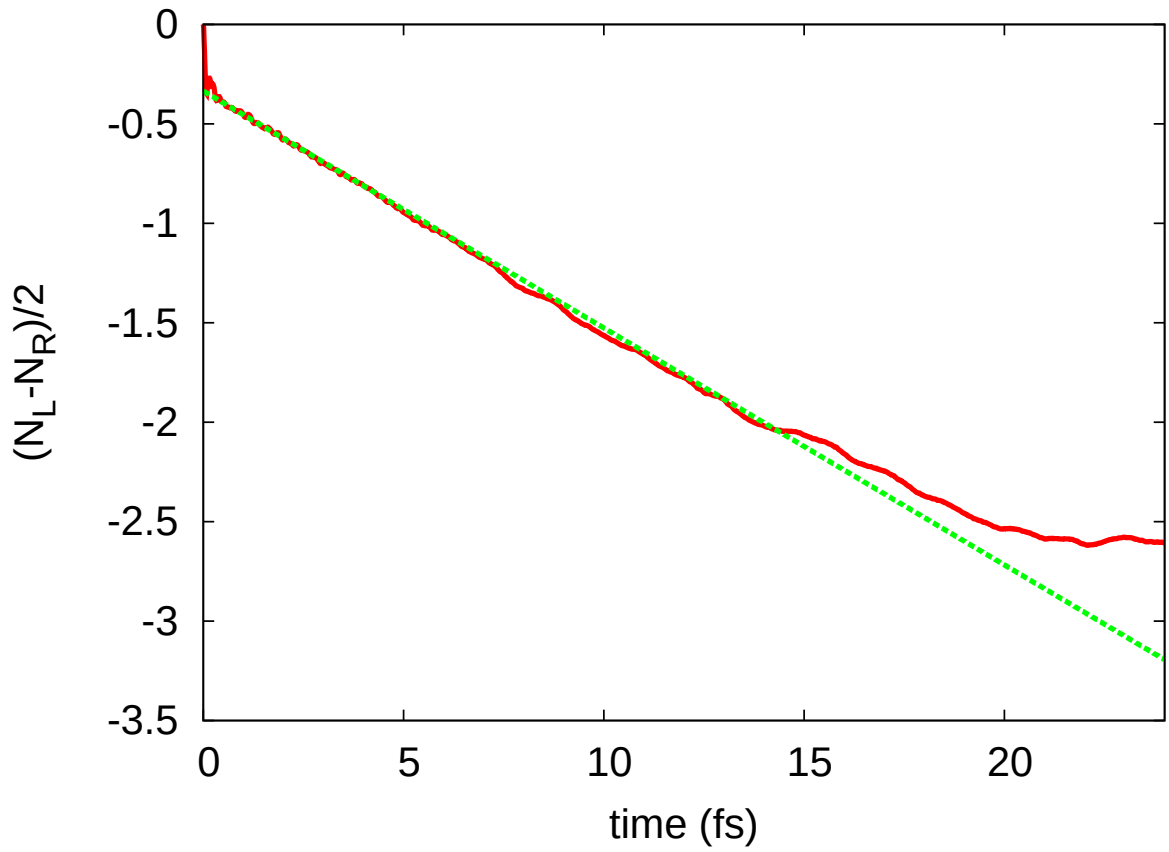
0
-0.5
-1
-1.5
-2
-2.5
-3
-3.5
0
5
10
15
20
time (fs)
(N_L-N_R)/2

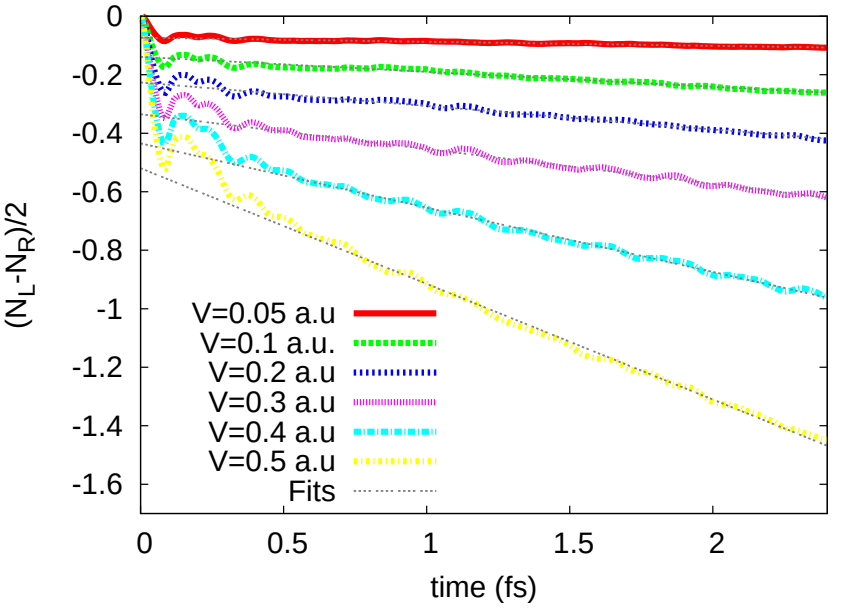
0
-0.2
-0.4
-0.6
-0.8
-1
-1.2
-1.4
-1.6
$(N_L-N_R)/2$
V=0.05 a.u
V=0.1 a.u.
V=0.2 a.u
V=0.3 a.u
V=0.4 a.u
V=0.5 a.u
Fits
0
0.5
1
1.5
2
time (fs)

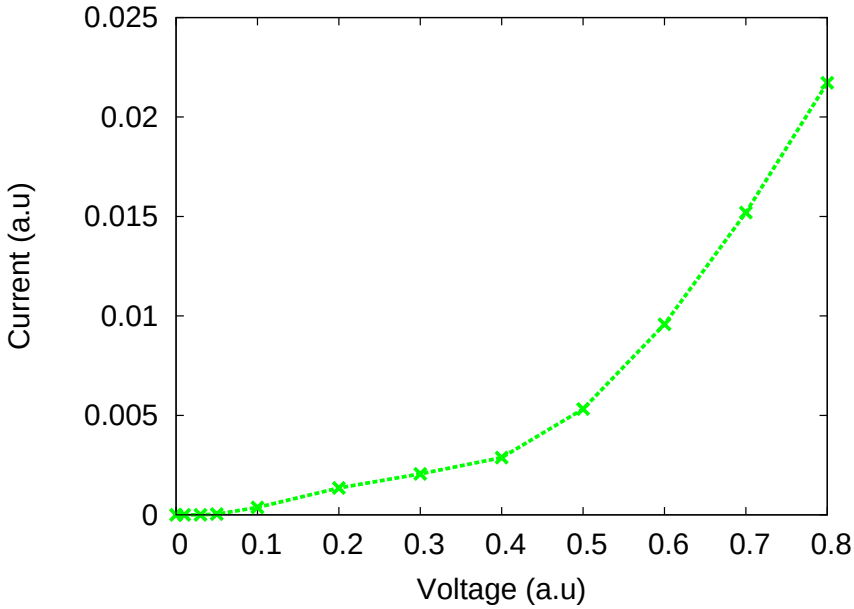
0.025
0.02
0.015
0.01
0.005
0
Current (a.u)
0
0.1
0.2
0.3
0.4
0.5
0.6
0.7
0.8
Voltage (a.u)

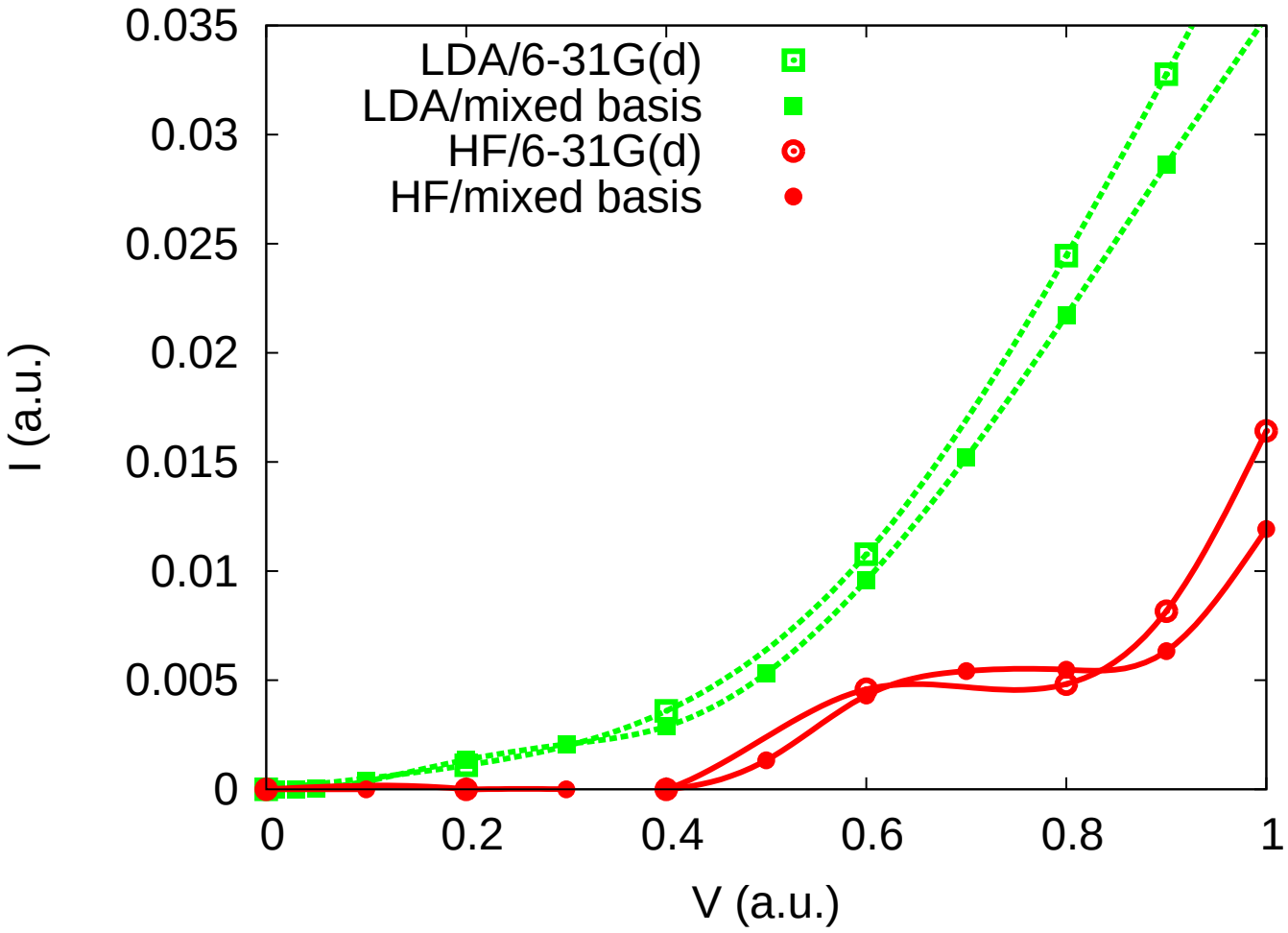
LDA/6-31G(d)
LDA/mixed basis
HF/6-31G(d)
HF/mixed basis
I (a.u.)
V (a.u.)
0.035
0.03
0.025
0.02
0.015
0.01
0.005
0
0
0.2
0.4
0.6
0.8
1

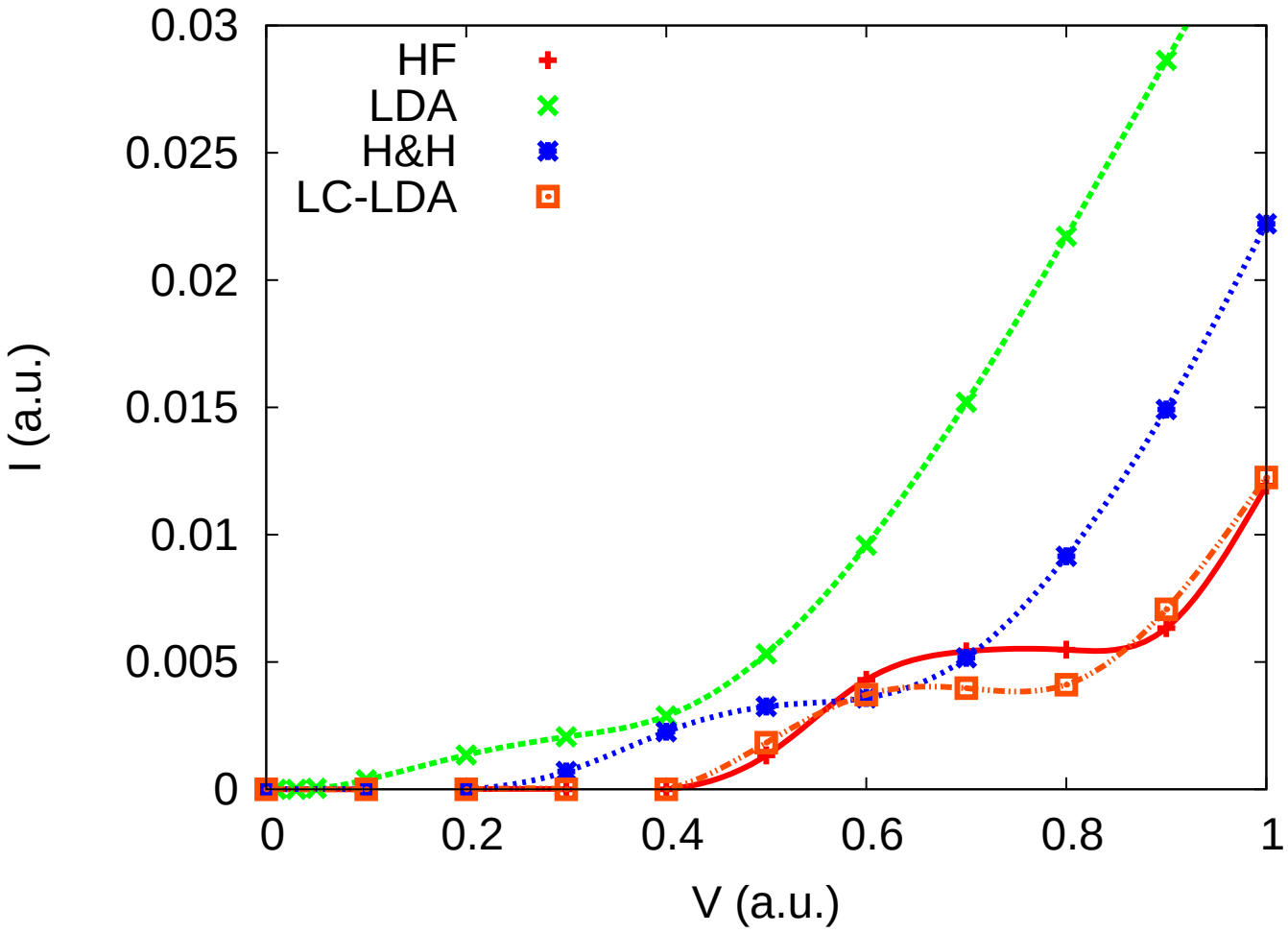
HF
LDA
H&H
LC-LDA
I (a.u.)
V (a.u.)
0.03
0.025
0.02
0.015
0.01
0.005
0
0
0.2
0.4
0.6
0.8
1

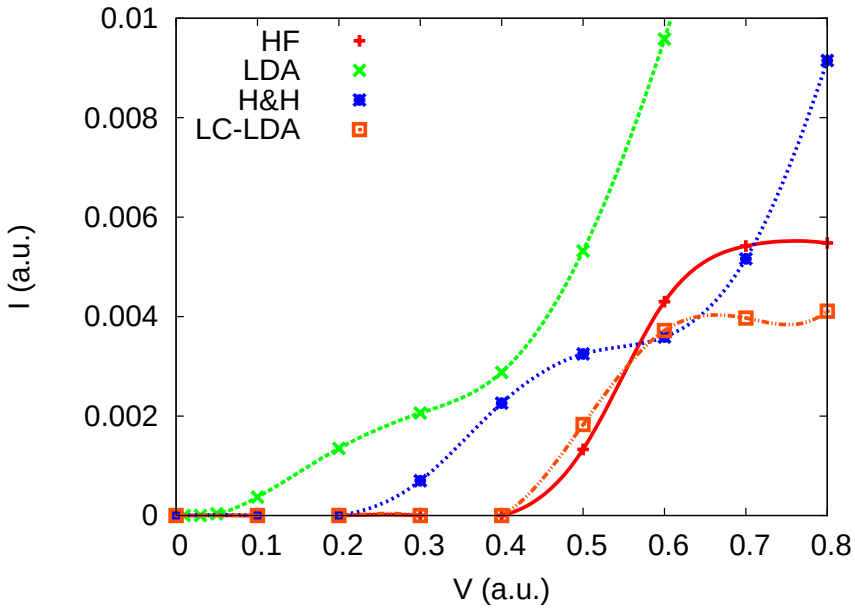
HF
LDA
H&H
LC-LDA
I (a.u.)
V (a.u.)
0.01
0.008
0.006
0.004
0.002
0
0
0.1
0.2
0.3
0.4
0.5
0.6
0.7
0.8

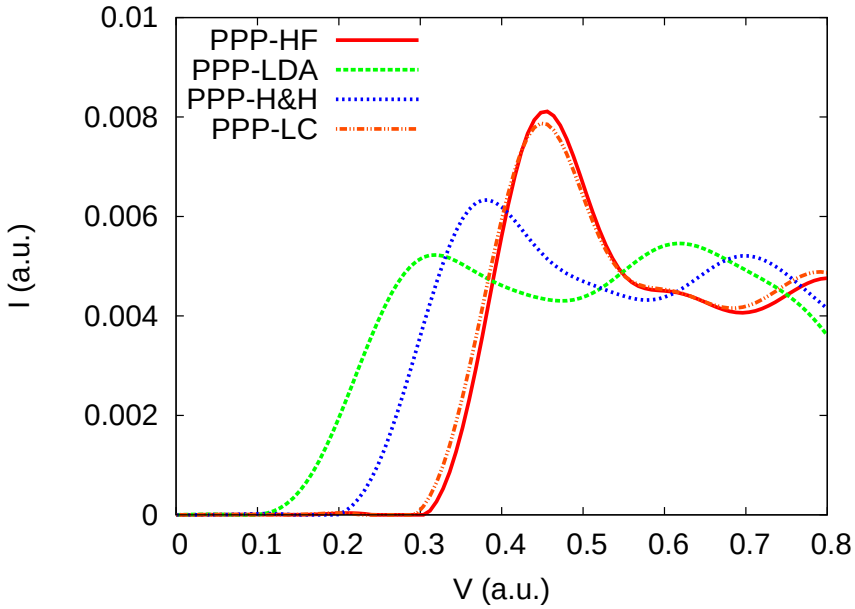
PPP-HF
PPP-LDA
PPP-H&H
PPP-LC
I (a.u.)
V (a.u.)
0.01
0.008
0.006
0.004
0.002
0
0
0.1
0.2
0.3
0.4
0.5
0.6
0.7
0.8

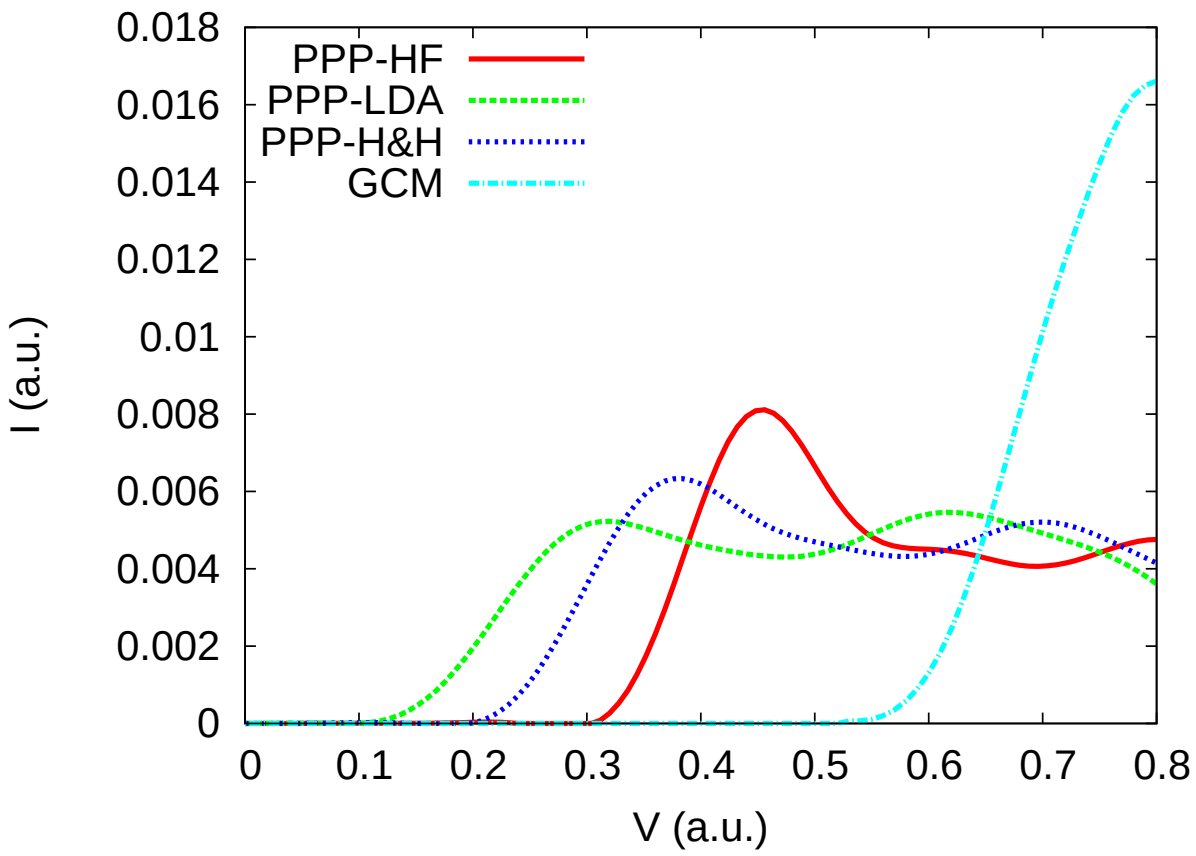
PPP-HF
PPP-LDA
PPP-H&H
GCM
I (a.u.)
V (a.u.)
0.018
0.016
0.014
0.012
0.01
0.008
0.006
0.004
0.002
0
0
0.1
0.2
0.3
0.4
0.5
0.6
0.7
0.8

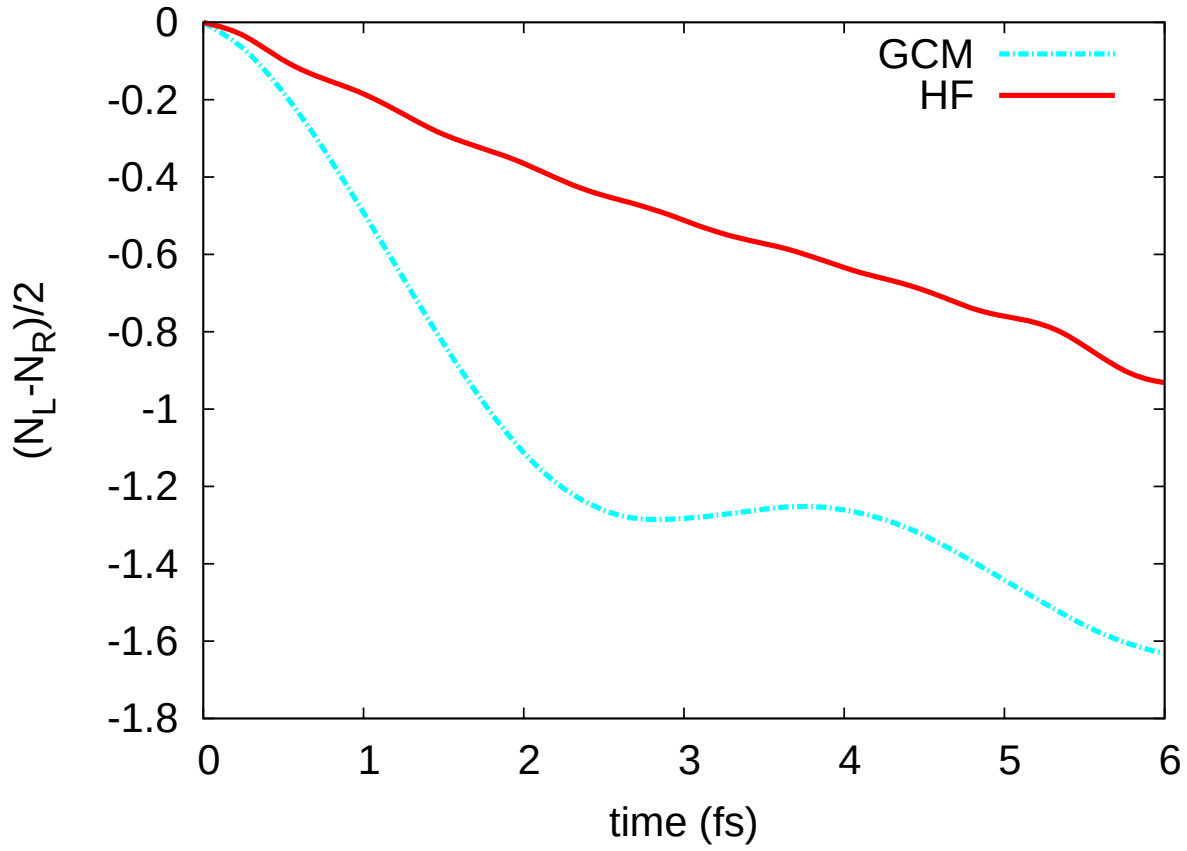
0
-0.2
-0.4
-0.6
-0.8
-1
-1.2
-1.4
-1.6
-1.8
0
1
2
3
4
5
6
time (fs)
(N_L-N_R)/2
GCM
HF